Suspended sediment source and propagation during monsoon events across nested sub-catchments with contrasted land uses in Laos

Sylvain Huon, O. Evrard, Elian Gourdin, Irène Lefèvre, Thierry Bariac, Jean-Louis Reyss, Thierry Henry Des Tureaux, Oloth Sengtaheuanghoung, Sophie Ayrault, Olivier Ribolzi

Journal of Hydrology: Regional Studies 9 (2017) 69–84

Contents lists available at ScienceDirect

Journal of Hydrology: Regional Studies

journal homepage: www.elsevier.com/locate/ejrh

Suspended sediment source and propagation during monsoon events across nested sub-catchments with contrasted land uses in Laos

Sylvain Huon[a,*], Olivier Evrard[b], Elian Gourdin[b], Irène Lefèvre[b], Thierry Bariac[c], Jean-Louis Reyss[b], Thierry Henry des Tureaux[d], Oloth Sengtaheuanghoung[e], Sophie Ayrault[b], Olivier Ribolzi[f]

[a] *Sorbonne Université UPMC Univ Paris 06, Institut d'Ecologie et des Sciences de l'Environnement de Paris (IEES Paris), Case 120, 4 Place Jussieu, 75252 Paris, Cedex 05, France*
[b] *Laboratoire des Sciences du Climat et de l'Environnement (LSCE), UMR 8212 (CEA-CNRS-UVSQ), Université Paris-Saclay, Domaine du CNRS, Avenue de la Terrasse, 91198 Gif-sur-Yvette Cedex, France*
[c] *Sorbonne Université UPMC Univ Paris 06, Institut d'Ecologie et des Sciences de l'Environnement de Paris (IEES Paris), CNRS, Campus INRA, AgroParisTech, Bâtiment EGER, 78550 Thiverval-Grignon, France*
[d] *IRD, National Agriculture and Forestry Research Institute (NAFRI), P.O. Box 4199, Ban Nogviengkham, Xaythany District, Vientiane, Lao Democratic People's Republic*
[e] *Department of Agricultural Land Management (DALaM), P.O. Box 4199, Ban Nogviengkham, Xaythany District, Vientiane, Lao Democratic People's Republic*
[f] *Géosciences Environnement Toulouse (GET), UMR 5563 (CNRS-UPS-IRD), 14 Avenue Edouard Belin, 31400 Toulouse, France*

ARTICLE INFO

Article history:
Received 23 July 2016
Received in revised form
26 November 2016
Accepted 28 November 2016

Keywords:
Suspended sediments
^{137}Cs
$^{210}Pb_{xs}$
^{7}Be
Total organic matter composition

ABSTRACT

Study region: Houay Xon catchment in northern Laos.
Study focus: Because agricultural headwater catchments of SE Asia are prone to erosion and deliver a significant proportion of the total suspended sediment supply to major rivers and floodplains, the potential sources of sediments and their dynamics were studied for two successive storm flow events in June 2013. Characterization of suspended sediment loads was carried out along a continuum of 7 monitoring stations, combining analyses of fallout radionuclides, particle borne organic matter and stream water properties.
New hydrological insights: Radionuclide activities showed that remobilization of soil particles deposited during the previous rainy season or supplied by riverbank erosion is the dominant process, although pulses of surface-soil derived sediments also propagate downstream. This interpretation is supported by suspended organic matter data that also fingerprints the mixing of surface soil *vs.* subsurface particles. The study moreover highlights the advantages and the drawbacks of combining fallout radionuclides, particle borne organic matter composition and stream water characteristics to discriminate and quantify sediment sources and dynamics in rural areas undergoing urban sprawl.

* Corresponding author at: Sorbonne Université UPMC Univ Paris 06, Institut d'Ecologie et des Sciences de l'Environnement de Paris (IEES Paris), Case 120, 4 Place Jussieu, Paris, Cedex 05, 75252, France.
E-mail address: sylvain.huon@upmc.fr (S. Huon).

http://dx.doi.org/10.1016/j.ejrh.2016.11.018

1. Introduction

Intense monsoon rainfalls may trigger severe erosion on cultivated or afforested hillslopes in small tropical mountainous catchments of SE Asia (Sidle et al., 2006; Valentin et al., 2008). Headwater catchments are characterized by high specific water discharges and sediment loads (Milliman and Syvitski, 1992) and may be considered as important sources of sediments to the floodplains of large rivers draining the region, such as the Mekong River (Lacombe et al., 2016). Furthermore, Southeast Asian rivers were also identified as major contributors of terrestrial organic matter supply to the ocean (Ludwig et al., 1996; Huang et al., 2012) and play a significant role in the global carbon cycle (Lal, 2003).

Fallout radionuclides can be used to understand the dynamics of suspended matter and sediment deposits in riverine environments (e.g., Matisoff et al., 2005; Olley et al., 2012, 2013). Beryllium-7 (^{7}Be; produced in the upper atmosphere) and unsupported lead-210 ($^{210}Pb_{xs}$; produced by the decay of radon-222 emitted by continental surfaces) are both mainly supplied to the soil surface by wet deposition (e.g., Caillet et al., 2001; Ioannidou and Papastefanou, 2006; Conaway et al., 2013). They are characterized by contrasted half-lives, 53.2 days and 22.3 years for ^{7}Be and ^{210}Pb, respectively, and by high solid − dissolved distribution coefficients (Olsen et al., 1985; Taylor et al., 2012). As they both bind strongly and rapidly to particles, they may be used to trace, during flood events, the source of fine suspended sediments from soils to deposition areas (Dominik et al., 1987; Bonniwell et al., 1999; Matisoff et al., 2002; Evrard et al., 2010; Saari et al., 2010). Furthermore, in tropical catchments where the summer monsoon is followed by a long dry period, the complete decay of ^{7}Be deposits occurs every year after the rainy season. It can then be assumed that most of the particles tagged with ^{7}Be at the onset of the monsoon are supplied to the rivers during the first storms of the rainy season. Discrimination between particles originating from surface soil and subsurface sources (gullies and riverbanks) can be achieved by comparing their activities in fallout cesium-137 (^{137}Cs) that was delivered by atmospheric nuclear bomb tests in the 1960s (Ritchie and McHenry, 1990). Measurable activities of ^{137}Cs (half-life of 30.2 years) are still found in surface soils whereas soil particles originating from gullies or riverbank collapses, sheltered from fallout radionuclides, are depleted in this radioisotope (Olley et al., 1993; Evrard et al., 2013; Hancock et al., 2014). In addition the composition of total organic matter (Kao and Liu, 2000; Masiello and Druffel, 2001; Bellanger et al., 2004; Huon et al., 2006; Hilton et al., 2010; Smith et al., 2013; Laceby et al., 2014) can also be used to trace changes in sources and pathways of particle borne organic matter across catchments (Ritchie and McCarty, 2003; Ellis et al., 2012; Schindler Wildhaber et al., 2012; Ben Slimane et al., 2013; Koiter et al., 2013; Laceby et al., 2016). To relate water flow to sediment transport, water characteristics such as its electric conductivity and ^{18}O content ($\delta^{18}O$) can also provide useful information on the contribution of overland flow and groundwater to river discharge (Nakamura, 1971; Pilgrim et al., 1979; Sklash and Farvolden, 1979; Ribolzi et al., 1996; Collins and Neal, 1998; Klaus and McDonnell, 2013).

Relevant information on soil sources of sediments in upstream catchments can be inferred from the study of suspended and dissolved load characteristics (Gourdin et al., 2014a, 2014b; Gourdin et al., 2015; Evrard et al., 2016). However, the nature of particulate matter may change further downstream, in particular, when land use involves areas affected by urban sprawl. Moreover linking soil sources to sediment delivery is not straightforward as deposition and remobilization processes take place, in particular, in lower parts of hillslopes (Chaplot and Poesen, 2012) and in ephemeral riverine depositional areas. The main objective of this study was to determine the contribution of cultivated soil surface and in-channel (subsurface) sources of particles in suspended sediment loads using a multi-tracer approach that combines fallout radionuclide activity measurements (^{137}Cs, $^{210}Pb_{xs}$ and ^{7}Be), total organic matter analyses (total organic carbon and total nitrogen concentrations, $\delta^{13}C$ and $\delta^{15}N$) and water flow characteristics (electrical conductivity and $\delta^{18}O$). These investigations were carried out in June 2013 for two successive storm flow events along the course of the Houay Xon river, flowing into the Mekong at Luang Prabang in Laos.

2. Study site

With an extension of 22 km^2 the Houay Xon (HX) catchment is located 10 km SE of Luang Prabang in northern Laos (Fig. 1). Its permanent stream is a tributary of the Nam Dong River, flowing into the Mekong River in Luang Prabang (Ribolzi et al., 2010). Its upstream basin, the Houay Pano (HP) catchment, is part of the MSEC (Monitoring Soil Erosion Consortium) network since 1998 (Valentin et al., 2008; Lacombe et al., 2016). The tropical monsoon climate of the region is characterized by the succession of dry and wet seasons, *ca.* 80% of annual rainfall (1302 ± 364 mm yr^{-1} on average between 1960 and 2013; Gourdin et al., 2014a) occurring during the rainy season from May to October (Ribolzi et al., 2008). The stream has an average base flow of 0.4 ± 0.1 L s^{-1} that may exceed 150 L s^{-1} at S4 during important flood events and flows into the Houay Xon (22.4 km^2 catchment) in the village of Ban Lak Sip (BLS).

The HX River is continuously monitored at station S10 (11.6 km^2 catchment), located 2.5 km downstream of the village. Additional sampling stations were installed, one within the BLS village (HP1; Fig. 1) and two further downstream along the HX River (HX2 and HX3 on Fig. 1). Another station, HT1, was added to monitor the Houay Thong (HT) tributary before its junction with the HX River, upstream of HX3 (Fig. 1). The characteristics of all the sampling stations and collection points are summarized in Table 1.

The geological basement of the Houay Xon catchment is composed at 95% by rocks of the lower Indonisian series (greywackes, pelites and quartzites; VKL, 1971), overlaid in the uppermost part of the catchment by Carboniferous – Permian limestone cliffs. Altitude ranges between 272 and 1300 m a.s.l. (Fig. 1). Soils consist of deep (>2 m) and moderately deep (>0.5 m) Alfisols (UNESCO, 1974), except along crests and ridges where Inceptisols can be also found (Chaplot et al.,

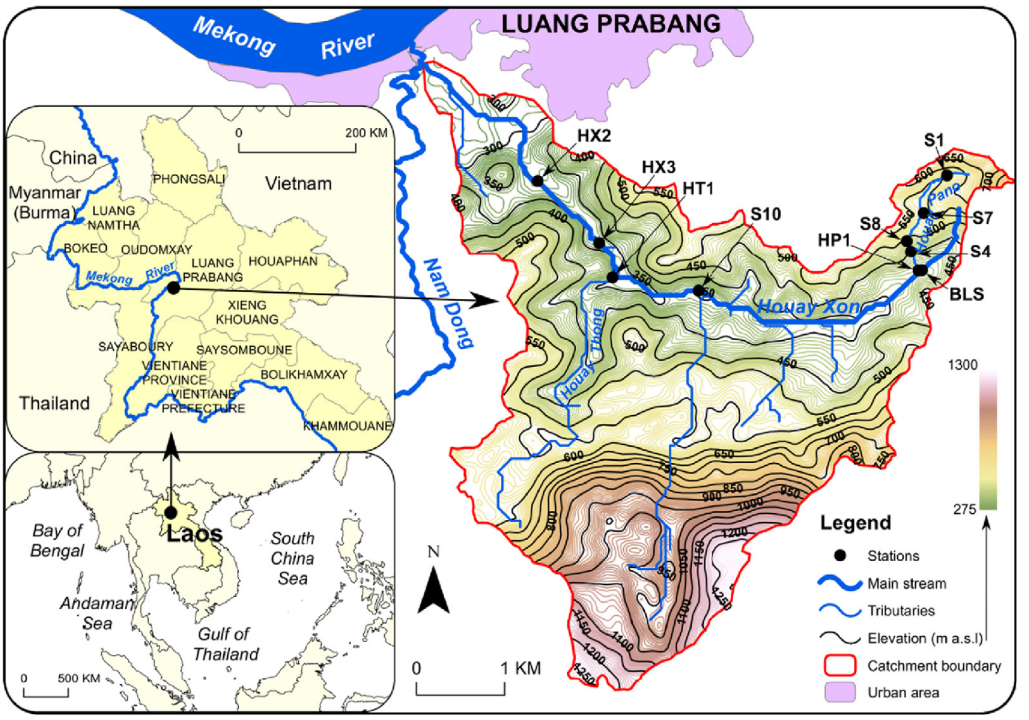

Fig. 1. Location of the Houay Xon catchment in Laos.

2009). Soils, devoid of carbonate minerals (Gourdin et al., 2015), have low cation exchange capacities and low pH ranging 4.9-5.5. In the Houay Xon catchment, native vegetation is lowland forest dominated by bamboos that was first cleared to implement shifting cultivation of upland rice at the end of the 1960s (Huon et al., 2013). Swampy areas are covered by Napier grass in the Houay Pano catchment and locally along the main stream at the outlet of Ban Lak Sip. As cultivation mainly takes place on steep slopes (3–150%, 61% on average), the Houay Pano catchment is very sensitive to soil erosion (Chaplot et al., 2005; Ribolzi et al., 2011; Patin et al., 2012; Chaplot and Poesen 2012). Due to the decline of soil productivity triggered by soil erosion over time and to an increasing need of labour to control weed invasion (Dupin et al., 2009), farmers have progressively replaced cultivated fields with teak plantations (Lacombe et al., 2016), which may grow on less fertile soils and provide income by tree logging after 10–12 years (Fig. 1). The main land uses over the catchment (Fig. 2) were primary and secondary forests (56%), cultivated lands (rice, maize and Job's tears, 23%), teak plantations (15%) and urban areas (6%). The downstream part of the Houay Xon catchment is connected to the suburban area of Luang Prabang where urban sprawl takes place on hillslopes connected to the river (Fig. 2). The evolution of stream water quality has been previously studied along the course of the HX river and revealed increasing releases of wastewater in downstream direction (Ribolzi et al., 2010).

Table 1
Characteristics of the sampling stations installed along the Houay Xon river.

Station*	Stream	Draining area (km^2)	Nature of samples[a]	Type of rainwater sampler	Type of river/OF sampler
S1	HP	0.20	SW	–	automatic pumping collector
S4	HP	0.60	SW	cumulative	automatic pumping collector
HP1	HP	1.15	SW	–	auto-capping collector
S10	HX	11.6	SW	fractionated	automatic pumping collector
HT1	HT	5.6	SW	–	auto-capping collector
HX3	HX	18.6	SW	cumulative	auto-capping collector
HX2	HX	19.8	SW	–	auto-capping collector
S7	hillslope	0.006	OF	–	manual collection
S8	hillslope	0.006	OF	–	manual collection
BLS	village	0.01	OF	–	auto-capping collector

* HP = Houay Pano, HX = Houay Xon, HT = Houay Thong (location on Fig. 1).
[a] SW = stream water and OF = overland flow.

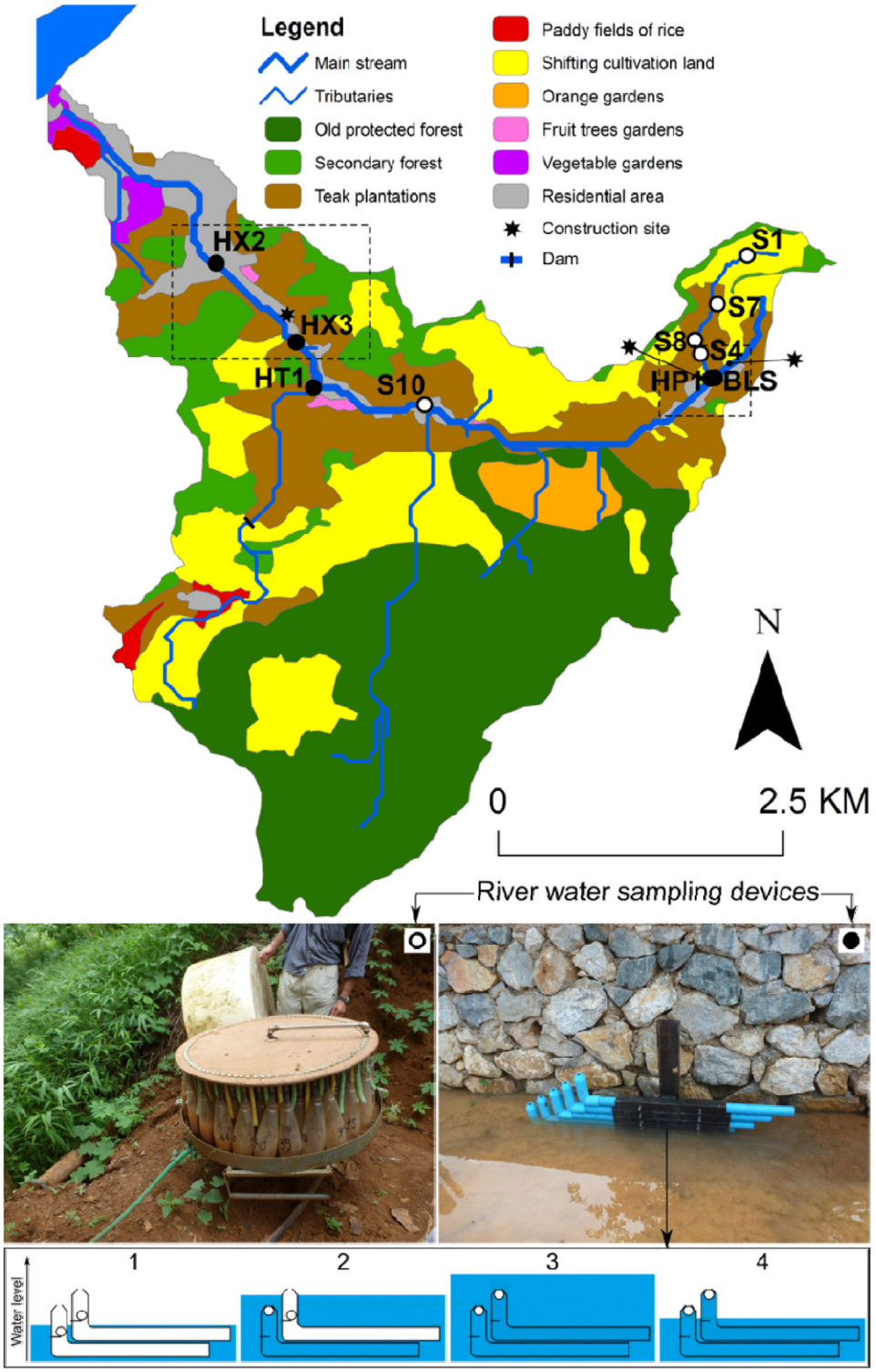

Fig. 2. Land use map of the catchment in 2012 and river water sampling devices installed at the different stations. Left picture: automatic pumping sampler; right picture: passive auto-capping collector (flood rise sampling). Bottom sketch: section views of the sampling stages of the passive auto-capping collector during water level rise (1–3) and decrease (4).

Table 2
Slope and estimated Manning's n coefficients used for discharge calculation at the passive collection stations.

Stations*	HP1	HT1	HX3	HX2
Slope	0.002	0.010	0.008	0.010
Manning's coefficient	0.040	0.056	0.029	0.022

* See Table 1 for description of the acronyms and Fig. 1 for station locations.

3. Materials and methods

3.1. Sampling and data collection

Rainfall, stream and overland flow water samples were collected during two storm flow events that occurred at the beginning of the rainy season on June 2 and June 4, 2013. The cumulated rainfall since the beginning of the year amounted to 332 mm for a total of 1742 mm in 2013. Rainfall intensity was monitored by an automatic tipping-bucket and by cumulative daily rain gauges. Stream water was collected by: (1) direct water uptake by automatic pumping samplers into plastic bottles at S4 and S10 after each 2-cm water level change above the defined flood threshold (Fig. 2); (2) passive collection during the flood rising stage at stations HP1, BLS, HT1, HX3 and HX2 (Fig. 2). The later collectors were made of *ca.* 1.3 L capacity superimposed tubes, installed along the river channel. They started filling with stream water once the level reached a fixed height and closed automatically by the means of an internal floating ball, preventing further mixing with overflowing river water (Fig. 2). Additional river water samples were collected manually during both the flood rise and the falling limb. Stream discharges were calculated from water level continuous records and rating curves at stations equipped with a gauging weir (S1, S4, S10) or estimated using Manning's equation (Manning, 1889 in Ferguson, 2010), for the sites equipped with passive auto-capping collectors using the following equation:

$$Q = (1/n) \times S^{1/2} \times A \times (A/P)^{2/3} \quad (1)$$

where Q is the water discharge ($m^3\ s^{-1}$); n is the Manning's roughness coefficient estimated for open channel flows following the method in Chow et al. (1988); S is the slope gradient (fractional number); A is the cross sectional area of flow (m^2) and P is the wetted perimeter (m). The values of S and n are summarized for each station in Table 2. Manning's coefficient typically varies between 0.012 for concrete to 0.100 for natural streams with heavy brush and timber.

The A and P values were determined for each corresponding water level (with 5 cm- height increments) using natural riverbed cross-sections. Stream discharge *vs.* water level relationships used at the passive collector stations were derived from continuous water level measurements by Schlumberger CTD-Diver® probes (Appendix A in Supplementary material).

Overall, 58 total suspended sediment samples (TSS) were collected, 53 at the 7 stations (S1, S4, HP1, S10, HT1, HX3 and HX2; Fig. 1) and 5 in a culvert installed along the main road in Ban Lak Sip (*ca.* 1 ha catchment). Samples were dried for 48 h at low temperature ($t \approx 50\ ^\circ C$) shortly after collection to avoid clay-bound organic matter breakdown. All results are reported in Appendix B in Supplementary material. Surface soil samples (0–10 cm soil depth or less, n = 65), previously collected using plastic trowels or density cylinders in the hillslopes connected to the Houay Pano Stream and the Houay Xon River (Huon et al., 2013; Gourdin et al., 2015) were considered in this study. Additional subsurface sources of sediments, namely gullies (n = 6) and riverbanks (n = 8), were sampled in December 2012.

3.2. Fallout radionuclide activity measurements

Total suspended sediments and rainwater sample treatments were conducted following the protocol detailed in Gourdin et al. (2014a, 2014b). Sample residues were placed in polypropylene tubes or packed into 15–60-mL polyethylene containers and sealed airtight to contain ^{222}Rn and allow in-growth of its decay products. Gamma spectrometry analyses were conducted at the Laboratoire des Sciences du Climat et de l'Environnement (LSCE) in Gif-sur-Yvette (France) for most samples and at the Laboratoire Souterrain de Modane (Reyss et al., 1995) for the smallest sediment samples (<4 g of dry matter), using low-background, high-efficiency, well-type or coaxial N- and P- type (Canberra Ortec®) GeHP detectors. Samples were analyzed within less than 53 days (^7Be half-life) after sampling. Counting time reached a maximum of *ca.* 9×10^4 s to minimize ^7Be decay during counting. Depending on the amount of sediment recovered, radionuclide activities were measured in individual or composite suspended sediment samples. The ^7Be, ^{137}Cs and ^{210}Pb activities were determined at 477.6 keV, 661.6 keV and 46.5 keV, respectively. The $^{210}Pb_{xs}$ activity was calculated by subtracting the supported activity from the total ^{210}Pb activity (measured at 46.5 keV) using two ^{226}Ra daughters, ^{214}Pb (average count at 295.2 and 351.9 keV) and ^{214}Bi (609.3 keV) (Le Cloarec et al., 2007). All measurements were corrected for background level determined every two months and for detector and geometry efficiencies. All activities were expressed in Bq kg^{-1} and were decay-corrected to the sampling date (June 2013). Counting efficiencies and reliability were checked using certified International Atomic Energy Agency (IAEA) standards prepared in the same containers as the samples. Efficiencies were interpolated for ^7Be energy. The uncertainty on radionuclide activity measurements averaged 16% for $^{210}Pb_{xs}$ and ^7Be and up to 34% for ^{137}Cs, depending on the amount of sample available, the counting time and the detector type.

Table 3
Average total organic matter composition and radionuclide activity in soils and sediments of the Houay Xon catchment.

Location	TOC (mgC g^{-1})	TN (mgN g^{-1})	TOC/TN	$\delta^{13}C$ (‰, PDB)	$\delta^{15}N$ (‰, AIR)	^{137}Cs (Bq kg^{-1})	$^{210}Pb_{xs}$ (Bq kg^{-1})
Surface soils (0–10 cm)	25 ± 5	2.1 ± 0.5	11.6 ± 2.0	−25.5 ± 1.4	6.7 ± 1.3	2.2 ± 0.9	38 ± 19
Stream banks	13 ± 6	1.1 ± 0.3	12.4 ± 7.7	−23.2 ± 4.4	8.6 ± 1.9	0.4 ± 0.3	14 ± 11
Gullies	14 ± 7	1.4 ± 0.6	9.6 ± 0.8	−22.7 ± 0.8	8.7 ± 2.1	0.4 ± 0.3	21 ± 27

Means ± 1 standard deviation. Data in Gourdin et al. (2014b, 2015).

The respective proportions of: (1) recently eroded sediment delivered during the event and labelled by rainfall radionuclides and, (2) surface soil particles labelled by ^{137}Cs, opposed to subsurface particles supplied by gullies and riverbanks were estimated in TSS load. The proportion of recently eroded sediment was determined following the method of Matisoff et al. (2005):

$$F = 100 \times [(A/B)/(A_0/B_0)] \quad (2)$$

where F is the percentage of recently eroded sediment, A and B are the ^{7}Be and $^{210}Pb_{xs}$ activities in TSS (Bq kg^{-1}) and A_0 and B_0 are the ^{7}Be and $^{210}Pb_{xs}$ activities in rainfall (Bq L^{-1}). A constant value of 6.2 for A_0/B_0 was used for F because a constant ^{7}Be: ^{210}Pb ratio was observed for the daily cumulative wet deposition both on June 2 and June 4 events (Gourdin et al., 2014a).

The proportion of surface soil – derived particles in each sediment sample was estimated using the equation proposed in Brigham et al. (2001) and Olley et al. (2012):

$$\alpha = 100 \times [(Cs_{sample} - Cs_{subsurf.})/(Cs_{surf.soil} - Cs_{subsurf.})] \quad (3)$$

where α is the percentage of particles derived from surface soil, Cs_{sample} is the ^{137}Cs activity in the sample, $Cs_{subsurf.}$ and $Cs_{surf.soil}$ are the mean ^{137}Cs activities in subsurface and surface soils, 0.4 ± 0.3 Bq kg^{-1} and 2.2 ± 1.9 Bq kg^{-1}, respectively (see Table 3 further in the text).

3.3. Total organic matter composition

Total suspended sediment samples were grounded with an agate mortar, weighed and packed into tin containers (5 × 9 mm). Total organic carbon (TOC) and total nitrogen (TN) concentrations, and stable C and N isotopes were measured using the Elementar® VarioPyro cube analyzer on line with a Micromass® Isoprime Isotope Ratio Mass Spectrometer (IRMS) facility at iEES-Paris. All samples were first analyzed for TOC and $\delta^{13}C$ using a set of tyrosine standards to calibrate TOC and TN concentrations and $\delta^{13}C$ measurements. When too low TN contents were obtained, a second run was performed on separate aliquots in order to optimize sample weight for $\delta^{15}N$ measurements. Oxygen for combustion was injected during 70 s (30 mL min^{-1}) and temperatures were set at 850 °C and 1120 °C for the reduction and combustion furnaces, respectively. Analytical precision was better than ± 0.1‰ *vs.* PDB and 0.2‰ *vs.* AIR standards (Coplen et al., 1983) for $\delta^{13}C$ and $\delta^{15}N$, respectively and ± 0.1 mg g^{-1} for TOC and TN. Data reproducibility was checked by replicate analyses of samples (50%) and of the tyrosine laboratory standard (Girardin and Mariotti, 1991). Due to the clayed and siliceous nature of soils and suspended sediments, no preliminary carbonate removal was required (Gourdin et al., 2015). Controls were made by adding a few drop of 10% HCl on selected samples. No visual CO_2 bubbling, typical for the dissolution of carbonate minerals, was observed.

3.4. Particle size distribution measurements

The particle size distribution of TSS was analyzed using the laser diffraction system (Malvern® Mastersizer 2000) coupled to a liquid dispersing unit (Hydro 2000G) available at Géosciences Paris-Sud lab (Université Paris-Sud, Orsay, France). The parameter chosen for comparison of the particle size distributions is d_{50}, the median diameter (μm) of sediment particles (Grangeon et al., 2012).

3.5. Water $\delta^{18}O$ and electrical conductivity measurements

Water sample aliquots were recovered in 30-mL glass flasks from stream, overland flow and rain, and filtered using <0.2 μm acetate filters. Stable oxygen isotope measurements were carried out using the standard CO_2 equilibration method (Epstein and Mayeda, 1953) and determined with a VG Optima® mass spectrometer (IEES-Paris, Thiverval Grignon, France). Isotopic ratios are reported using the $\delta^{18}O$ notation, relative to the Vienna-Standard Mean Ocean Water (V-SMOW, Gonfiantini, 1978) with an analytical precision better than ± 0.1‰. Water electric conductivity (EC) was monitored every 6-mn at the inlet of each gauging station using in situ CTD-Diver® probes. Complementary measurements were performed with an YSI® 556 probe on water samples.

4. Results and interpretation

4.1. Storm flow characteristics

Four successive storms took place between June 2 and 4. They were characterized by variable rainfall intensities (for a detailed description see in Gourdin et al., 2014a) and triggered two successive low intensity flood events that propagated downstream in the Houay Xon catchment (Fig. 3). At four stations located downstream of nearby residential areas (i.e. HP1, S10, HX3 and HX2, Fig. 1 and 2), daily cyclic variations of river EC were observed as a consequence of variable wastewater releases into the channel. For two of these stations (S10 and HX3), pulses of high EC (>1000 $\mu S\,cm^{-1}$) occurred during base flow, resulting from intermittent releases by a fruit juice factory located just upstream of S10. They were removed in order to focus on the study of the evolution of EC during the flood events. The river water EC evolved during the two floods (Fig. 4) as the result of varying contributions of event water (EW) and pre-event water (PEW) to total water discharge (Gourdin et al., 2014b). Groundwater (GW), characterized by high EC (350–550 $\mu S\,cm^{-1}$), typically supplies stream water during base flow (PEW) whereas rainwater with very low EC (mainly below the detection limit of the conductivity meter) has a dilution effect during the floods. Most of EW was supplied by overland flow (OF) that displayed intermediate EC values, 20–150 $\mu S\,cm^{-1}$, controlled by interactions between runoff water and surface soil particles along catchment's slopes (Gourdin et al., 2015). However, in most cases OF is characterized by low EC, *ca.* 20 $\mu S\,cm^{-1}$. As a consequence, mixing between GW and OF supplied stream water compositions with typically decreasing patterns (down to 100–200 $\mu S\,cm^{-1}$), related to the dilution of PEW base flow by OF (Fig. 4) and initiated during the water rising stage. River water $\delta^{18}O$ ranged −9.5–−4.1‰ (Fig. 4). These values suggest a higher ^{18}O content for PEW and a lower ^{18}O content for EW during the period of maximum rainfall intensity of the June 2 storm and during the second and third storms on June 4 (Gourdin et al., 2014a).

Rainclouds moved in SE direction across HT1 and HX3 drainage areas. Afterwards, they continued in upstream direction over the catchment and reached successively S10, HP1, S4 and S1 (Fig. 3). Most discharge peaks involved a large supply of OF water, as illustrated by the opposite evolution of EC and discharge. However, the dilution trend is thoroughly reduced downstream (at HT1, HX3, HX2; Fig. 4), in particular during the second flood of June 4, indicating that the contribution of soil water and groundwater was enhanced compared to the pattern observed in the upper catchment. These events most likely corresponded to OF originating from the hillslopes directly connected to the main channel.

Three successive storms triggered flood events on June 4. During the first event that occurred during the night, cumulative rainfall amounted *ca.* 5-mm resulting in limited rises of water level at the gauging stations (Fig. 4).

The increase of water discharge at all stations was almost synchronous. The second storm took place 12 h later and was followed less than 3 h after by a third event (Fig. 3). During these two storms, rainclouds moved from S10 towards S1, as shown by the relative increase of rainfall intensity (Gourdin et al., 2014a). In contrast to June 2, rainfall did not start earlier at HX2, suggesting a SW origin of the related air masses. The successive peaks of water discharge reached higher levels than during the June 2 event at all stations with the exception of HX2 (Fig. 3).

4.2. Suspended sediment transport during storm flows

4.2.1. Total suspended sediment load and particle size distribution

The TSS loads ranged 0.2–27.7 $g\,L^{-1}$ (Appendix B in Supplementary material). As for water discharge, the highest values were recorded at downstream stations during both floods (HT1, HX2 and HX3, Fig. 5). Suspended loads first increased during the water rising stage and quickly decreased near peak flow (S4, HP1, S10, HT1 and HX3, Fig. 5). This behaviour was mainly observed during the June 4 event and reflected a clockwise hysteresis pattern, as shown for the upper catchment in 2012 by Gourdin et al. (2014b). The median size of suspended particles ranged between 6 and 24 μm, showing the preferential transport of fine sediments by these low intensity floods. Except for HX2, the highest d_{50} values were recorded during the June 4 storm. At S4, S10 and HX3, d_{50} values decreased at peak flow. In other words, finer particles were associated with higher discharges and TSS loads.

4.2.2. Fallout radionuclide activity in suspended sediment loads

The fallout radionuclide activities in TSS are reported in Appendix B in Supplementary material and their temporal evolution is plotted on Fig. 6. Maximum activities reached $234 \pm 18\,Bq\,kg^{-1}$ for ^{7}Be (first discharge peak at S10 on June 2), $85 \pm 20\,Bq\,kg^{-1}$ for $^{210}Pb_{xs}$ (main discharge peak at S4 on June 4) and $3.1 \pm 1.3\,Bq\,kg^{-1}$ for ^{137}Cs (main discharge peak at S4 on June 4). Half of the TSS loads displayed low ^{137}Cs activities (below 0.5 $Bq\,kg^{-1}$) suggesting that the contribution of subsurface sources to suspended loads, dominated during both floods, in particular in the downstream areas. High ^{137}Cs activities (>1.5 $Bq\,kg^{-1}$), reflecting high contributions of particles derived from soil surface layers, were only measured at upstream stations S4, HT1 and HX3 on June 4 during the first and second discharge peaks.

The $^{210}Pb_{xs}$ activities of suspended sediments at S4 were high and increased with Q and TSS load during the rising stage of the June 4 flood (Fig. 6). Similarly, $^{210}Pb_{xs}$ evolved together with Q and TSS at HX2 during the same flood. In contrast, decreasing trends were observed at HX3 during both events and at HT1 during the June 2 event.

The ^{7}Be activities strongly varied during both flood events. On June 2, several samples displayed values above 100 $Bq\,kg^{-1}$ (including all S10 samples) and only one showed an activity lower than 50 $Bq\,kg^{-1}$. In contrast, all suspended sediment samples collected during the second flood displayed low activities below 100 $Bq\,kg^{-1}$ including 13 samples with activities

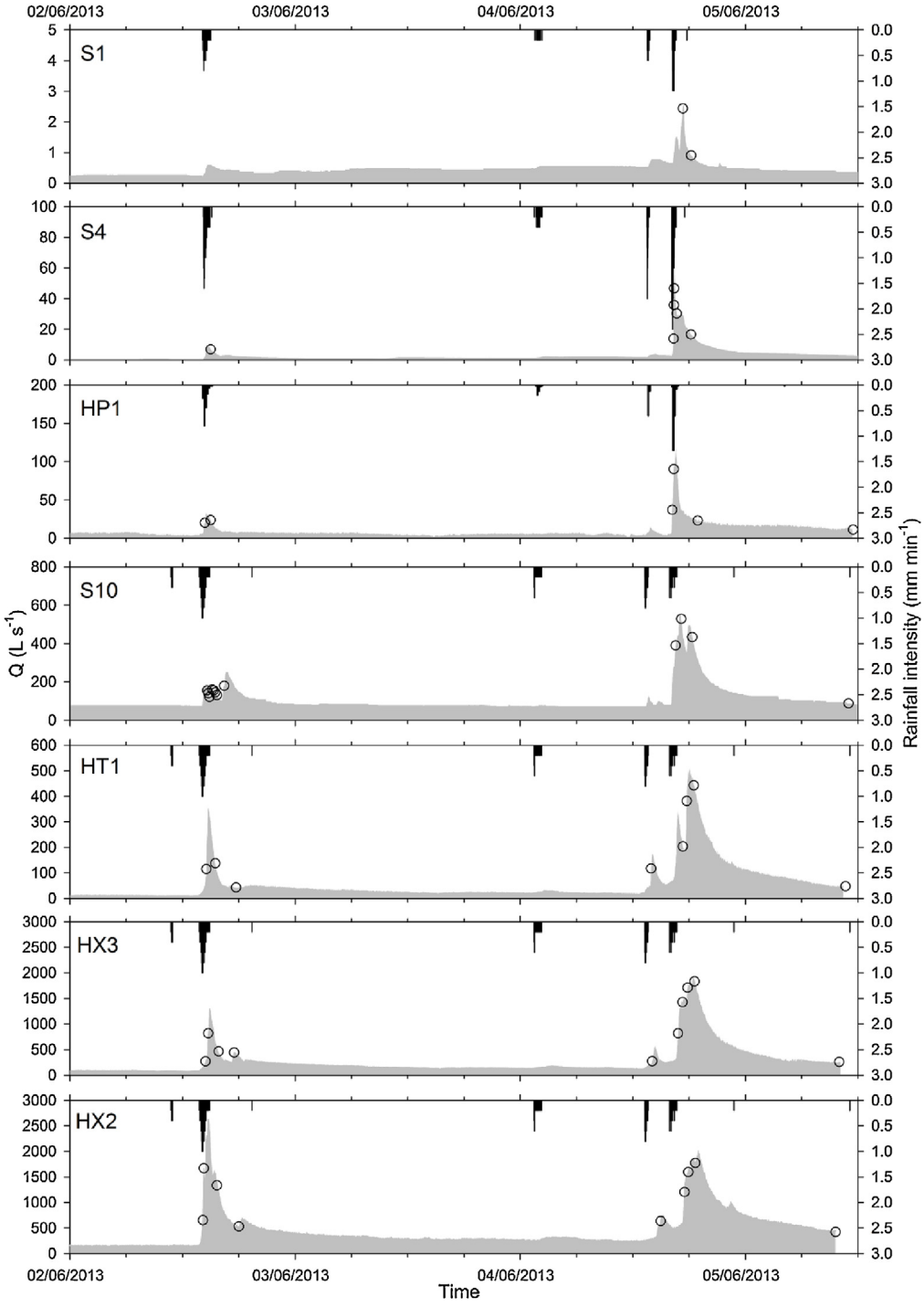

Fig. 3. Rainfall intensity (I, black bars), Houay Xon water discharge (Q, shaded area) and water samples collection time (open circles) during the June 2 and 4 floods at each station along the HX continuum (location in Fig. 1). For HT1, HX3 and HX2 rainfall intensity is that recorded at S10. Note the different Q scales.

below 50 Bq kg^{-1}. This behaviour may be related to ^{7}Be wet deposition that was almost twice lower on June 4 than on June 2 at S10, 6.0 ± 0.1 *vs.* 11.6 ± 1.0 Bq m^{-2}, respectively, despite similar cumulative rainfall records for both floods (Gourdin et al., 2014a). Different fallout radionuclide evolution patterns were observed at the successive stations during each flood. At S10, HT1 and HX3 on June 2, ^{7}Be and $^{210}Pb_{xs}$ activities decreased throughout the event, a behaviour consistent with the decreasing trends observed for both radionuclides in rainwater during the same event (Gourdin et al., 2014a). The collection

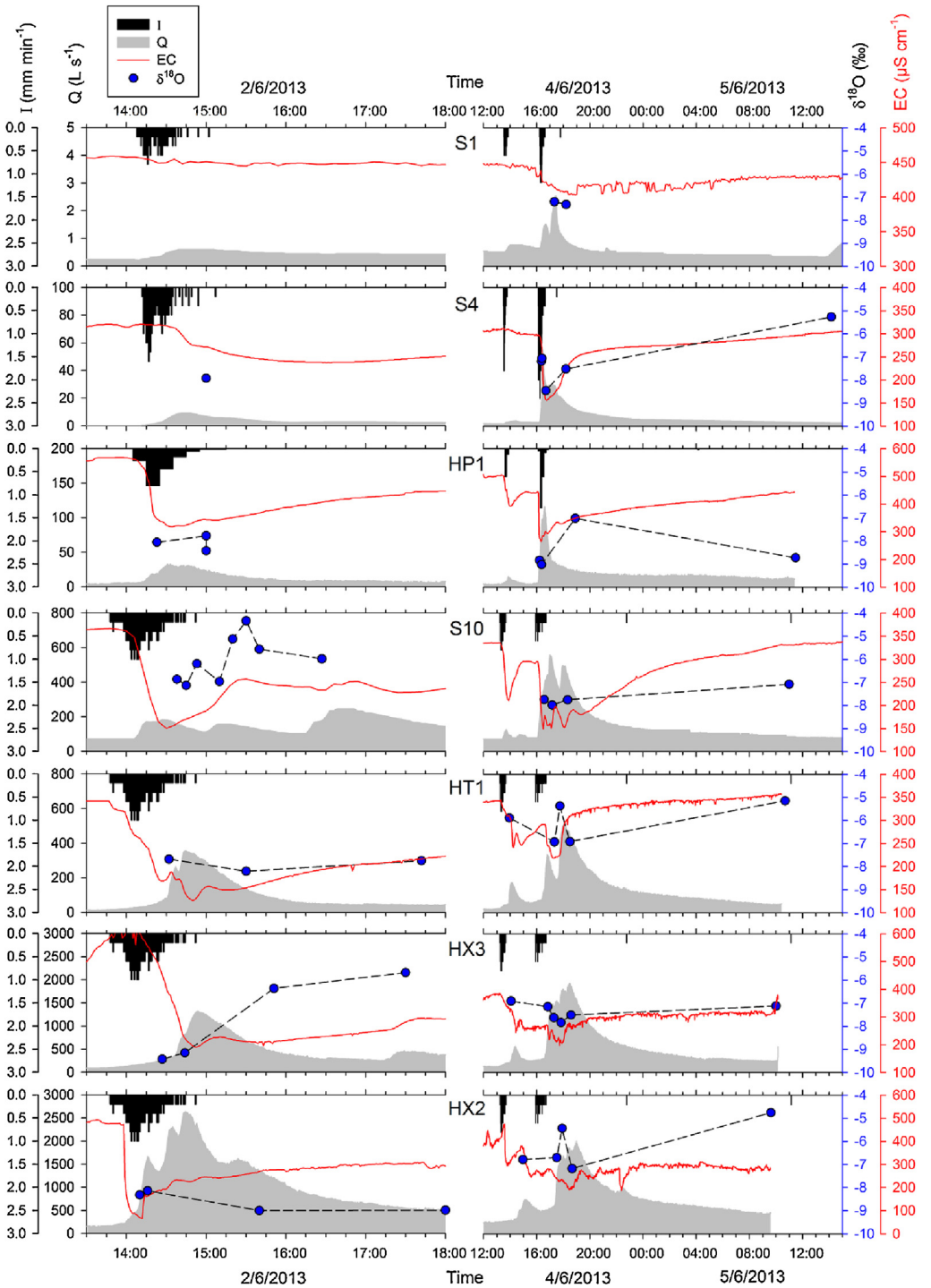

Fig. 4. Stream water $\delta^{18}O$ (filled circles and dashed line) and water electric conductivity (EC, solid line) records during the June 2 and 4 floods at each station (location in Fig. 1). Shaded areas represent water discharge (Q), vertical bars rainfall intensity (I) at each station, except at HT1, HX3 and HX2, where the rainfall data recorded at S10 were used. Note the different Q and EC scales in each plot and the different time scales for each flood.

of particles with high ^{7}Be activities reflects the transport of sediments labelled by the previous rainfall events that occurred at the beginning of the 2013 monsoon. Furthermore, ^{7}Be displayed larger variations upstream, whereas dilution of recently eroded particles (high ^{7}Be content) by remobilized particles (depleted in ^{7}Be) was likely observed downstream. The particles collected at all stations on June 5, i.e. the day following the second flood, displayed low fallout radionuclide activities (Fig. 6).

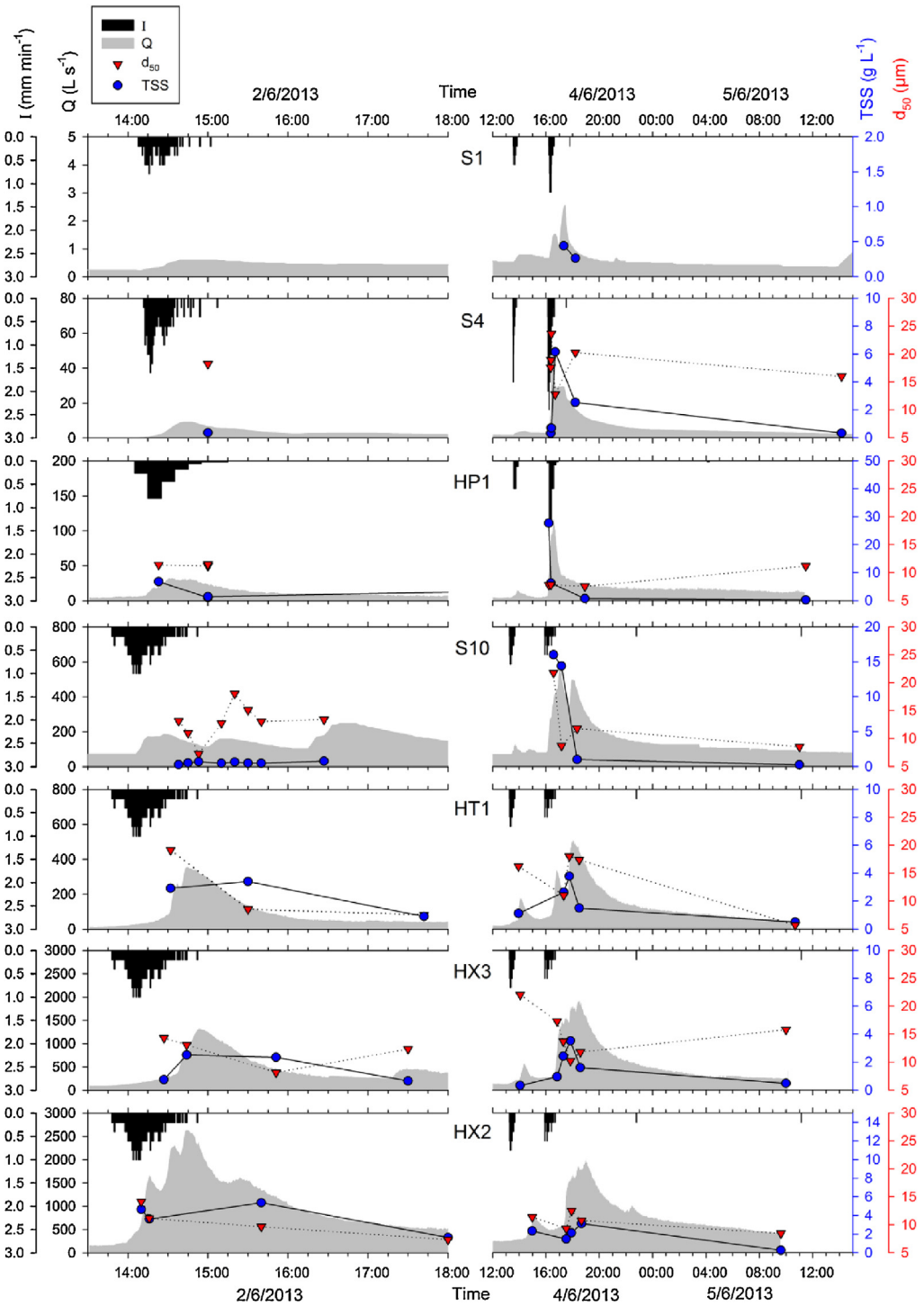

Fig. 5. Total suspended sediment loads (TSS, filled circles) and particle size distributions (d_{50}, triangles) during the June 2 and 4 floods at each station (location in Fig. 1). Shaded areas represent water discharge (Q), vertical bars rainfall intensity (I) at each station, except at HT1, HX3 and HX2 where rainfall data recorded at S10 were used. Note the different Q and TSS scales in each plot and the different time scales for each flood.

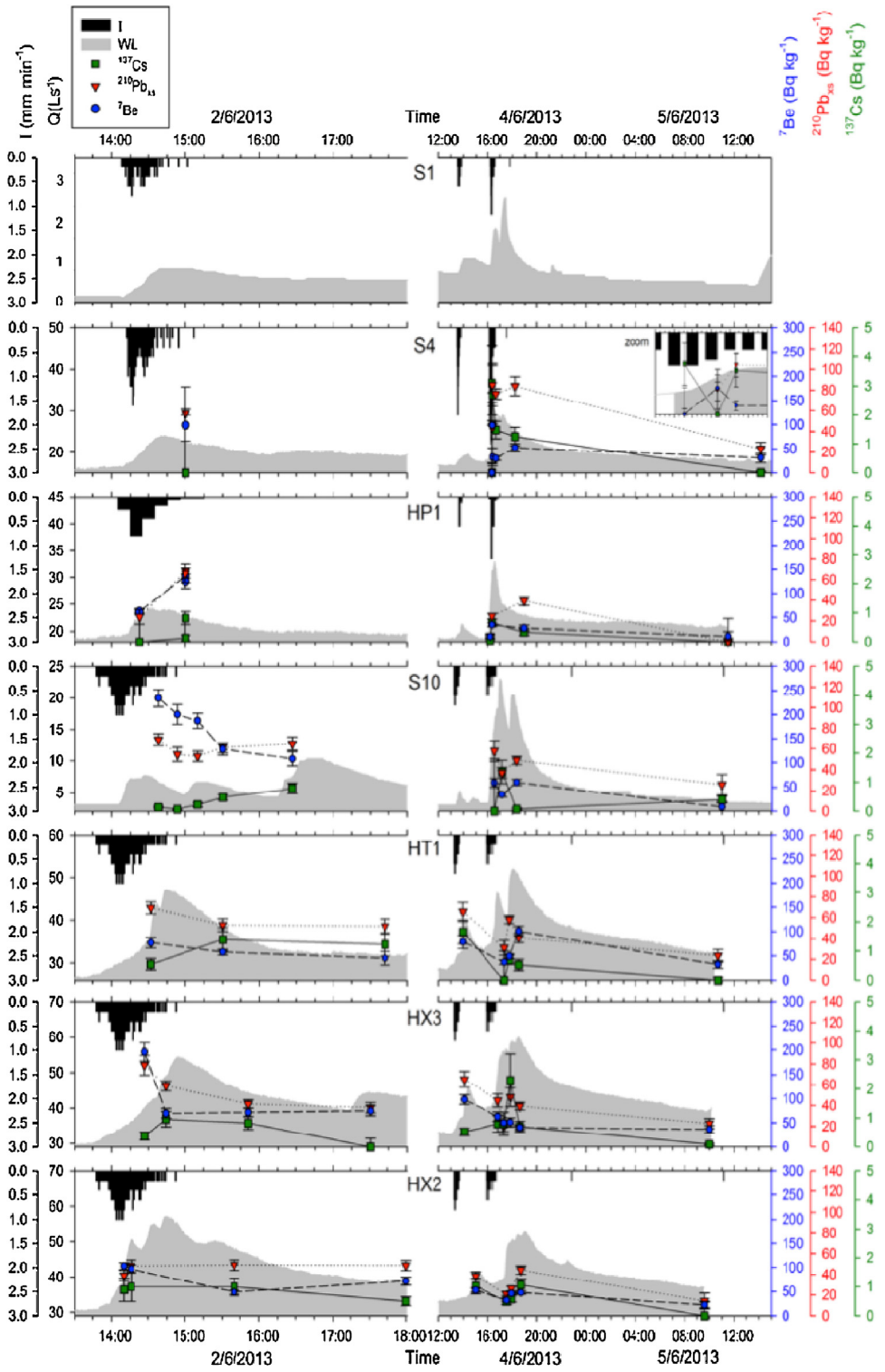

Fig. 6. Fallout radionuclide activities (^{7}Be, filled circles; ^{210}Pb$_{xs}$, triangles; ^{137}Cs, squares) in TSS loads collected during the June 2 and 4 floods at each station (location in Fig. 1). Shaded areas represent water discharge (Q), vertical bars rainfall intensity (I) at each station, except at HT1, HX3 and HX2 where S10 data were used. Note the different Q scales and the different time scales for each flood.

4.3. Composition of suspended organic matter

The composition of particle borne organic matter in TSS (TOC and TN concentrations, TOC/TN, $\delta^{13}C$ and $\delta^{15}N$) is reported in Appendix B in Supplementary material. The TOC concentrations ranged between 8 and 129 mgC g^{-1}. More than half of the samples are enriched in TOC compared to the average concentration of 25 ± 5 mgC g^{-1} reported for surface soils of the catchment (Table 3). The TOC concentration decreases with soil depth to averages of 14.8 ± 4.7 mgC g^{-1} and 12.1 ± 4.2 mgC g^{-1} at 10–20 cm and 20–30 cm soil depths, respectively (Huon et al., 2013). The $\delta^{13}C$ increases with soil depth to -24.0 ± 1.3‰ at 20–30 cm. Accordingly, soil particles originating from subsurface sources should be depleted in TOC and enriched in ^{13}C (as well as in ^{15}N) with respect to surface soil derived material.

In upper parts of the catchment (S1, S4, HP1) and downstream (S10) their temporal evolution during the floods is consistent with the observations made during the study of a previous flood, in 2012 (Gourdin et al., 2015). Suspended loads are characterized by varying suspended organic matter compositions. Most of the changes took place during the discharge peaks, during which TOC concentration, TOC/TN and $\delta^{13}C$ in TSS loads decreased towards the average composition of surface soil-derived organic matter at S1 and S4. Further downstream the $\delta^{13}C$ values were higher than in the upper parts of the catchment, which reflects both the input of C4-plant derived organic matter originating from swamps covered with Napier grass along the HX course (Huon et al., 2013) and of subsurface particles supplied by channel banks and gullies (Table 3). Half of suspended sediments collected downstream (Appendix B in Supplementary material) displayed $\delta^{13}C$ values above −24‰. These two potential sources of suspended organic matter could not be separated except for S1 where Napier grass grows within the main channel just upstream of the station. The enhanced supply of weakly mineralized organic matter (i.e., vegetation debris) is illustrated by increasing TOC/TN values. Ratios in the range 9–14 are typical for surface soil organic matter in the catchment (11.6 ± 2.0; Table 3) whereas channel banks display a wider range of values, associated with the different types of organic matter deposited in the channel during water level decrease. It can be noticed that high supplies of weakly degraded vegetation debris should also be characterized by low $\delta^{15}N$ (Gourdin et al., 2015). At peak flow most $\delta^{15}N$ values in suspended sediments shifted to *ca.* 7–8‰, in the range of the surface soil (6.7 ± 1.3‰, Table 3) and subsurface (8.6 ± 1.9‰, Table 3) pools. Only a few low values, down to 2‰, clearly support the major contribution of weakly mineralized organic matter at S4, S10 and HT1 (Appendix B in Supplementary material).

5. Discussion

With a return period of less than 1 year (Bricquet et al., 2003), the two flood events studied were representative of the common rainfall conditions prevailing during the rainy season in northern Laos. Although low rainfall intensities were observed, early monsoon events may, nevertheless, be responsible for significant sediment yields because: 1) they take place when soil surfaces are still sparsely covered by vegetation and, 2) they remobilize sediment deposits along stream banks and in river channels and swampy areas. Surface soil is the dominant potential source of particles for cultivated areas in the upper catchment parts. In contrast sediment remobilization processes are expected to play a key role in downstream areas (Gourdin et al., 2014b). Mixing between these two potential sources of suspended sediments can be inferred from radionuclide activity measurements with the α and F parameters (Fig. 7). Total suspended sediment loads in streams draining cultivated sub-catchments (S4, HP1 and HT1) are characterized by lower sediment yields (below *ca.* 200 g s^{-1}). They can be distinguished from those collected downstream along the main river channel (above *ca.* 200 g s^{-1}; S10, HX2 and HX3). The former display variable proportions of recently eroded (*ca.* $0 < F < 40\%$) fine suspended sediments (*ca.* $10 < d_{50} < 25$ μm) originating, to a large extent, from the surface soil of these sub-catchments (*ca.* $40 < \alpha < 100\%$). In contrast, the later display a lower contribution of surface soil ^{137}Cs-enriched particles (*ca.* $\alpha < 40\%$) with an equivalent or even higher proportion of recently eroded particles labelled by $^{7}Be/^{210}Pb_{xs}$ (*ca.* $0 < F < 60\%$). High F and low α values reflect higher occurrences of ^{7}Be-labelled subsurface particles depleted both in ^{137}Cs and in $^{210}Pb_{xs}$ and also result from the exposure of collapsed riverbanks to recent radionuclide deposition by rainfall (Olley et al., 2013; Laceby et al., 2014). The smaller particle size of the corresponding TSS loads ($d_{50} \approx 10$–12 μm) is best explained by particle sorting processes that take place during suspended transport in the river, i.e., local deposition of coarser particles due to decreases in flow velocity. In addition, runoff flowing on deeper soil layers exhausted at construction sites (i.e., Nelson and Booth, 2002) also likely supplied fine subsurface particles depleted in ^{137}Cs, particularly in the downstream section of the main HX channel (Fig. 2).

The composition of particle borne organic matter in samples with low sediment content (below *ca.* 200 g s^{-1}) also corresponded to surface soil sources that are characterized by high TOC contents (3–13 mgC g^{-1}, Fig. 8), high TOC:TN ratios (>12, Fig. 8), relatively low $\delta^{15}N$ (<6‰, Fig. 8) and variable $\delta^{13}C$ values (*ca.* −20‰ to −27‰ in Fig. 8). The ^{13}C-depleted samples are consistent with surface soil organic matter supply derived from land under shifting cultivation of upland rice and teak plantations at S4 (C3-dominant vegetation cover in the Houay Pano catchment, Fig. 2) whereas the ^{13}C-enriched samples may reflect mixed C3-C4 vegetation covers in the HT catchment (Fig. 2). However, the input of subsurface particles can also provide ^{13}C-enriched particle borne organic matter from deep soil layers. Indeed, the composition of soil organic matter often displays ^{13}C- and ^{15}N-enrichment patterns with depth (up to 1–3‰), associated with selective mineralization or organic compounds (e.g., Desjardins et al., 1994; Boström et al., 2007; Rumpel and Kögel-Knabner, 2011), which could explain the observed trends.

The large variability observed is also controlled by the dynamics of TSS supply during the flood events and involves the mixing of recently eroded soil surface particles, originating from cultivated soils, and soil surface particles previously

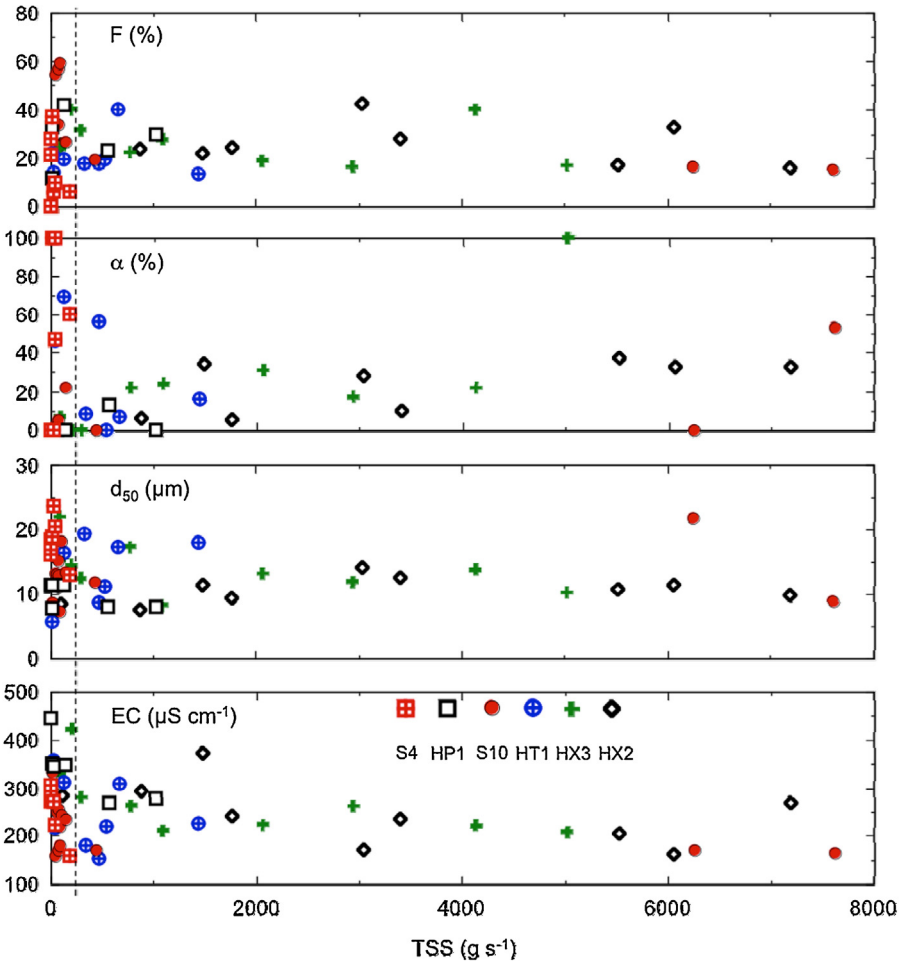

Fig. 7. Relations between total suspended sediment (TSS) flux and the proportion of recently eroded sediment (F), the proportion of surface soil-derived particles (α), the median particle size diameter (d_{50}) and the water electrical conductivity (EC) in TSS loads sampled during the June 2 and 4 floods at 6 stations along the HX continuum (location in Fig. 1). The dashed lines separate TSS with very low sediment yields at *ca.* 200 g s^{-1}.

deposited in the channels that are remobilized and exported downstream during the floods. When plotted against TSS flux, the evolution of TOC content, TOC/TN, $\delta^{13}C$ and $\delta^{15}N$ display typical hyperbolic like trends (Fig. 8) that have been interpreted in different ways. They can either be explained by an enhanced contribution of particulate "fossil" organic matter supplied by an increasing mechanical erosion of the geological basement of the riverbed during storm flows (Meybeck, 2006; Copard et al., 2007; Clark et al., 2013) or by the evolution of TSS loads towards the "average" composition of soils in the catchment with intensifying soil erosion and sediment transport (Ludwig et al., 1996). They can alternatively reflect the dilution of particle borne organic matter by in-channel or allochthonous mineral matter supply (Gourdin et al., 2015). The first interpretation does not match our data as only low intensity erosive events occurred. With high sediment deliveries $\delta^{15}N$ increased to *ca.* 6–9‰ (Fig. 8) but low values are rather expected for the contribution of "fossil organic matter", often displaying the signature of buried vegetation residues (Huon et al., 2006). Except for TOC, the supply of sediments with a typical subsurface $\delta^{13}C$, $\delta^{15}N$ and TOC/TN signature corresponding either to particles originating from subsoil layers and exported by gullies or remobilized matter from river channels (Table 3), better matches with the observed trends. However, no significant correlation directly links radionuclide activities and total organic matter composition and only mixing patterns were observed. In addition, the contribution of fine subsoil particles, impoverished in organic matter, supplied by exhausted soils at construction sites, could have further diluted the TOC concentration of TSS loads in downstream sections without significantly changing the isotopic composition of suspended organic matter.

6. Conclusions

Monitoring suspended sediment loads with fallout radionuclide activities and total organic matter elemental and stable isotopic compositions during two successive low intensity floods at the beginning of the rainy season across a network of nested sub-catchments along the Houay Xon River in Northern Laos provided information on sediment sources and

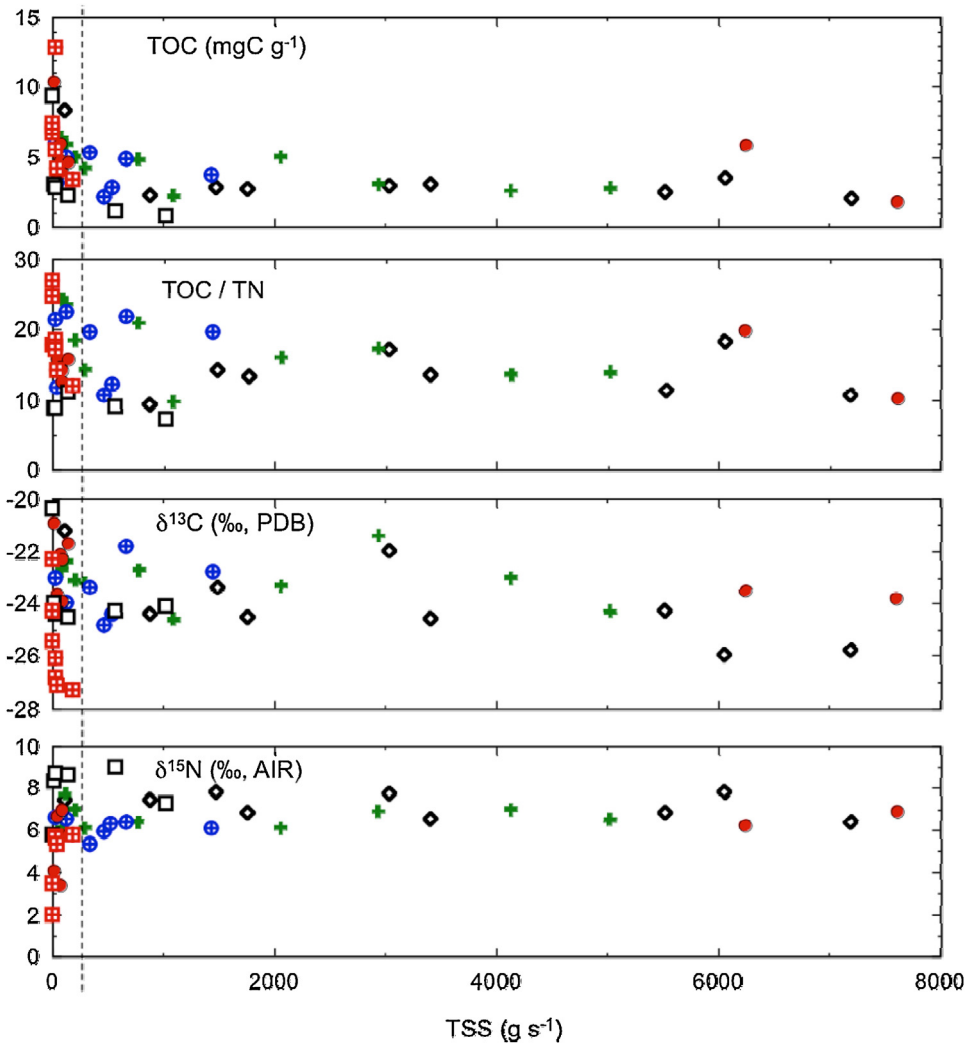

Fig. 8. Relations between total suspended sediment (TSS) flux and total organic carbon concentration (TOC), TOC/TN ratio, $\delta^{13}C$ and $\delta^{15}N$ of particle borne organic matter in TSS loads sampled during the June 2 and 4 floods at 6 stations along the HX continuum (location in Fig. 1). The dashed lines separate TSS with very low sediment yields at *ca*. 200 g s^{-1}. Same legend as in Fig. 7.

propagation. In upper catchment parts most sediment originated from the surface layers of cultivated soils. Further downstream, mixed contributions of surface (recently eroded surface soil particles) and subsurface (in-channel remobilization and riverbank erosion) particle sources dominated. In addition suspended loads also likely involved the contribution of recently eroded subsurface particles supplied by runoff from exhausted soil layers at construction sites. Overall, the data showed that, during low intensity storm flow events, the source of suspended sediments along the course of this tropical mountainous river was mainly controlled by land use and by the connectivity of hillslopes to the mainstream channel.

Conflict of interest

No conflict of interest.

Acknowledgements

The authors would like to thank the Lao NAFRI (National Agriculture and Forestry Research Institute in Vientiane), the MSEC project (Multi-Scale Environmental Changes) and French Institut de Recherche pour le Développement (IRD) for their support. They are also grateful to Keo Oudone Latsachack, Bounsamai Soulileuth and Chanthamousone Thammahacksa for their help in the field. Thanks to Christophe Colin and Olivier Dufaure (UMR Géosciences Paris-Sud, Université Paris Sud, Orsay) for their help with particle size distribution measurements, to Patricia Richard and Véronique Vaury (iEES-Paris, Thiverval Grignon and Paris, France) for conducting EA-IRMS measurements. Elian Gourdin received a PhD fellowship

from the Université Paris-Sud. This work received financial support from the French CNRS INSU initiative structurante EC2CO/BIOHEFECT (Belkong project) and ANR Teciteasy project (ANR-13-AGRO-0007).

Appendix A. Supplementary data

Supplementary data associated with this article can be found, in the online version, at http://dx.doi.org/10.1016/j.ejrh.2016.11.018 .

References

Bellanger, B., Huon, S., Velasquez, F., Vallès, V., Girardin, C., Mariotti, A., 2004. Monitoring soil organic carbon erosion with $\delta^{13}C$ and $\delta^{15}N$ on experimental field plots in the Venezuelan Andes. Catena 58, 125–150.

Ben Slimane, A., Raclot, D., Evrard, O., Sanaa, M., Lefèvre, I., Ahmadi, M., Tounsi, M., Rumpel, C., Ben Mammou, A., Le Bissonnais, Y., 2013. Fingerprinting sediment sources in the outlet reservoir of a hilly cultivated catchment in Tunisia. J. Soils Sediments 13, 801–815.

Bonniwell, E.C., Matisoff, G., Whiting, P.J., 1999. Determining the times and distances of particle transit in a mountain stream using fallout radionuclides. Geomorphology 27, 75–92.

Boström, B., Comstedt, D., Ekblad, A., 2007. Isotope fractionation and ^{13}C enrichment in soil profiles during the decomposition of soil organic matter. Oecologia 153, 89–98.

Bricquet, J.-P., Boonsaner, A., Bouahom, B., Toan, T.D., 2003. Statistical analysis of long series rainfall data: a regional study in South-East Asia. In: Maglinao, A.R., Valentin, C., Penning de Vries, F. (Eds.), From Soil Research to Land and Water Management: Harmonizing People and Nature: Proceedings of the IWMI-ADB Project Annual Meeting and 7th MSEC Assembly. LAOS, Vientiane, pp. 83–89.

Brigham, M.E., McCullough, C.J., Wilkinson, P., 2001. Analysis of suspended-sediment concentrations and radioisotope levels in the Wild Rice River Basin, Northwestern Minnesota. 1973-98, US. Geological Survey Water Resources Investigations Report 01-4192, pp. 21.

Caillet, S., Arpagaus, P., Monna, F., Dominik, J., 2001. Factors controlling ^{7}Be and ^{210}Pb atmospheric deposition as revealed by sampling individual rain events in the region of Geneva, Switzerland. J. Environ. Radioact. 53, 241–256.

Chaplot, V., Poesen, J., 2012. Sediment, soil organic carbon and runoff delivery at various spatial scales. Catena 88 (1), 46–56.

Chaplot, V., Rumpel, C., Valentin, C., 2005. Water erosion impact on soil and carbon redistributions within uplands of Mekong River. Glob. Biogeochem. Cycles 19, http://dx.doi.org/10.1029/2005GB002493.

Chaplot, V., Podwojewski, P., Phachomphon, K., Valentin, C., 2009. Soil erosion impact on soil organic carbon spatial variability on steep tropical slopes. Soil Sci. Soc. Am. J. 73 (3), 769–779.

Chow, V.T., Maidment, D.R., Mays, L.W., 1988. Applied hydrology. In: McGraw-Hill Int. Eds. Civil Engineering Series. McGraw-Hill Book Co, Singapore (572 p).

Clark, K.E., Hilton, R.G., West, A.J., Malhi, Y., Gröcke, D.R., Bryant, C.L., Ascough, P.L., Robles Caceres, A., New, M., 2013. New views on old carbon in the Amazon river: insight from the source of organic carbon eroded from the Peruvian Andes. Geochem. Geophys. Geosyst. 14, 1644–1659.

Collins, R.U., Neal, C., 1998. The hydrochemical impacts of terraced agriculture, Nepal. Sci. Total Environ. 212, 233–243.

Conaway, C.H., Storlazzi, C.D., Draut, A.E., Swarzenski, P.W., 2013. Short-term variability of ^{7}Be atmospheric deposition and watershed response in a Pacific coastal stream Monterey Bay, California, USA. J. Environ. Radioact. 120, 94–103.

Copard, Y., Amiotte-Suchet, P., Di-Giovanni, C., 2007. Storage and release of fossil organic carbon related to weathering of sedimentary rocks. Earth Planet. Sci. Lett. 258, 345–357.

Coplen, T.B., Kendall, C., Hoople, J., 1983. Comparison of stable isotope reference samples. Nature 302, 236–238.

Desjardins, T., Andreux, F., Volkoff, B., Cerri, C.C., 1994. Organic carbon and ^{13}C contents in soils and soil size- fractions, and their changes due to deforestation and pasture installation in eastern Amazonia. Geoderma 61, 103–118.

Dominik, J., Burrus, D., Vernet, J.-P., 1987. Transport of the environmental radionuclides in an alpine watershed. Earth Planet. Sci. Lett. 84 (2–3), 165–180.

Dupin, B., de Rouw, A., Phantahvong, K.B., Valentin, C., 2009. Assessment of tillage erosion rates on steep slopes in northern Laos. Soil Tillage Res. 103 (1), 119–126.

Ellis, E.E., Keil, R.G., Ingalls, A.E., Richey, J.E., Alin, S.R., 2012. Seasonal variability in the sources of particulate organic matter of the Mekong river as discerned by elemental and lignin analyses. J. Geophys. Res. 117 (G1) (G01038).

Epstein, S., Mayeda, T., 1953. Variation of ^{18}O content of waters from natural sources. Geochim. Cosmochim. Acta 4 (5), 213–224 (1953).

Evrard, O., Némery, J., Gratiot, N., Duvert, C., Ayrault, S., Lefèvre, I., Poulenard, J., Prat, C., Bonté, P., Esteves, M., 2010. Sediment dynamics during the rainy season in tropical highland catchments of central Mexico using fallout radionuclides. Geomorphology 124 (1–2), 42–54.

Evrard, O., Poulenard, J., Némery, J., Ayrault, S., Gratiot, N., Duvert, C., Prat, C., Lefèvre, I., Bonté, P., Esteves, M., 2013. Tracing sediment sources in a tropical highland catchment of central Mexico by using conventional and alternative fingerprinting methods. Hydrol. Process. 27 (6), 911–922.

Evrard, O., Laceby, P., Huon, S., Lefèvre, I., Sengtaheuanghoung, O., Ribolzi, O., 2016. Combining multiple fallout radionuclides (^{137}Cs, ^{7}Be, $^{210}Pb_{xs}$) to investigate temporal sediment source dynamics in tropical, ephemeral riverine systems. J. Soils Sediments 16, 1130–1144.

Ferguson, R., 2010. Time to abandon the Manning equation? Earth Surf. Process. Landforms 35 (15), 1873–1876.

Girardin, C., Mariotti, A., 1991. Analyse isotopique du ^{13}C en abondance naturelle: un système automatique avec robot préparateur. Cah. Orstom, sér. Pédol. XXVI 120, 371–380.

Gonfiantini, R., 1978. Standards for stable isotope measurements in natural compounds. Nature 271, 534–536.

Gourdin, E., Evrard, O., Huon, S., Reyss, J.-L., Ribolzi, O., Bariac, T., Sengtaheuanghoung, O., Ayrault, S., 2014a. Spatial and temporal variability of ^{7}Be and ^{210}Pb wet deposition during four successive monsoon storms in a catchment of northern Laos. J. Environ. Radioact. 136, 195–205.

Gourdin, E., Evrard, O., Huon, S., Lefèvre, I., Ribolzi, O., Reyss, J.-L., Sengtaheuanghoung, O., Ayrault, S., 2014b. Suspended sediment dynamics in a Southeast Asian mountainous catchment: combining river monitoring and fallout radionuclide analyses. J. Hydrol. 519, 1811–1823.

Gourdin, E., Huon, S., Evrard, O., Ribolzi, O., Bariac, T., Sengtaheuanghoung, O., Ayrault, S., 2015. Sources and export of particle-borne organic matter during a monsoon flood in a catchment of northern Laos. Biogeosciences 12, 1073–1089.

Grangeon, T., Legout, C., Esteves, M., Gratiot, N., Navratil, O., 2012. Variability of the particle size of suspended sediment during highly concentrated flood events in a small mountainous catchment. J. Soils Sediments 12, 1549–1558.

Hancock, G.J., Wilkinson, S.N., Hawdon, A.A., Keen, R.J., 2014. Use of fallout tracers ^{7}Be, ^{210}Pb and ^{137}Cs to distinguish the form of sub-surface soil erosion delivering sediment to rivers in large catchments. Hydrol. Process. 28, 3855–3874.

Hilton, R.G., Galy, A., Hovius, N., Horng, M.-J., Chen, H., 2010. The isotopic composition of particulate organic carbon in mountain rivers of Taiwan. Geochim. Cosmochim. Acta 74, 3164–3181.

Huang, T.-H., Fu, Y.-H., Pan, P.-Y., Chen, C.-T.A., 2012. Fluvial carbon fluxes in tropical rivers. Curr. Opin. Environ. Sustain. 4, 162–169.

Huon, S., Bellanger, B., Bonté, P., Sogon, S., Podwojewski, P., Girardin, C., Valentin, C., de Rouw, A., Velasquez, F., Bricquet, J.-P., Mariotti, A., 2006. Monitoring soil organic carbon erosion with isotopic tracers: two case studies on cultivated tropical catchments with steep slopes (Laos, Venezuela). In: Roose, E.J., Lal, R., Feller, C., Barthès, B., Stewart, B.A. (Eds.), Soil Erosion and Carbon Dynamics. CRC Press, Boca Raton. Florida (USA), pp. 301–328.

Huon, S., de Rouw, A., Bonté, P., Robain, H., Valentin, C., Lefèvre, I., Girardin, C., Le Troquer, Y., Podwojewski, P., Sengtaheuanghoung, O., 2013. Long-term soil carbon loss and accumulation in a catchment following the conversion of forest to arable land in northern Laos. Agric. Ecosyst. Environ. 169, 43–57.

Ioannidou, A., Papastefanou, C., 2006. Precipitation scavenging of ^{7}Be and ^{137}Cs radionuclides in air. J. Environ. Radioact. 85 (1), 121–136.
Kao, S.J., Liu, K.K., 2000. Stable carbon and nitrogen isotope systematics in a human- disturbed watershed (Lanyang-Hsi) in Taiwan and the estimation of biogenic particulate organic carbon and nitrogen fluxes. Glob. Biogeochem. Cycles 14, 189–198.
Klaus, J., McDonnell, J.J., 2013. Hydrograph separation using stable isotopes: review and evaluation. J. Hydrol. 505, 47–64.
Koiter, A.J., Owens, P.N., Petticrew, E.L., Lobb, D.A., 2013. The behavioural characteristics of sediment properties and their implications for sediment fingerprinting as an approach for identifying sediment sources in river basins. Earth Sci. Rev. 125, 24–42.
Laceby, J.P., Olley, J., Pietsch, T.J., Sheldon, F., Bunn, S.E., 2014. Identifying subsoil sediment sources with carbon and nitrogen stable isotope ratios. Hydrol. Process. 29 (8), 1956–1971.
Laceby, J.P., Huon, S., Onda, Y., Vaury, V., Evrard, O., 2016. Do forests represent a long-term source of contaminated particulate matter in the Fukushima Prefecture? J. Environ. Manage. 183, 742–753.
Lacombe, G., Ribolzi, O., de Rouw, A., Pierret, A., Latsachak, K., Silvera, N., Pham Dinh, R., Orange, D., Janeau, J.-L., Soulileuth, B., Robain, H., Taccoen, A., Sengphaathith, P., Mouche, E., Sengtaheuanghoung, O., Tran Duc, T., Valentin, C., 2016. Contradictory hydrological impacts of afforestation in the humid tropics evidenced by long-term field monitoring and simulation modelling. Hydrol. Earth Syst. Sci. 20, 2691–2704.
Lal, R., 2003. Soil erosion and the global carbon budget. Environ. Int. 29, 437–450.
Le Cloarec, M.-F., Bonté, P., Lefèvre, I., Mouchel, J.-M., Colbert, S., 2007. Distribution of ^{7}Be, ^{210}Pb and ^{137}Cs in watersheds of different scales in the Seine River basin: inventories and residence times. Sci. Total Environ. 375, 125–139.
Ludwig, W., Probst, J., Kempe, S., 1996. Predicting the oceanic input of organic carbon by continental erosion. Glob. Biogeochem. Cycles 10, 23–41.
Manning, R., 1889. On the flow of water in open channels and pipes. Trans. Inst. Civ. Eng. Irel. 20, 161–207.
Masiello, C.A., Druffel, E.R.M., 2001. Carbon isotope geochemistry of the Santa Clara river. Glob. Biogeochem. Cycles 15, 407–416.
Matisoff, G., Bonniwell, E.C., Whiting, P.J., 2002. Radionuclides as indicators of sediment transport in agricultural watersheds that drain to lake Erie. J. Environ. Qual. 31, 62–72.
Matisoff, G., Wilson, C.G., Whiting, P.J., 2005. The ^{7}Be/^{210}Pb$_{xs}$ ratio as an indicator of suspended sediment age or fraction new sediment in suspension. Earth Surf. Process. Landforms 30 (9), 1191–1201.
Meybeck, M., 2006. Origins and behaviors of carbon species in world rivers, in soil erosion and carbon dynamics. In: Roose, E.J., Lal, R., Feller, C., Barthès, B., Stewart, B.A. (Eds.), Soil Erosion and Carbon Dynamics. CRC Press, Boca Raton. Florida (USA), pp. 209–238.
Milliman, J.D., Syvitski, J.P.M., 1992. Geomorphic/tectonic control of sediment discharge to the ocean: the importance of small mountainous rivers. J. Geol. 100 (5), 525–544.
Nakamura, R., 1971. Runoff analysis by electrical conductance of water. J. Hydrol. 14, 197–212.
Nelson, E.J., Booth, D.B., 2002. Sediment sources in an urbanistic, mixed land-use watershed. J. Hydrol. 264, 51–68.
Olley, J.M., Murray, A.S., Mackenzie, D.H., Edwards, K., 1993. Identifying sediment sources in a gullied catchment using natural and anthropogenic radioactivity. Water Resour. Res. 29, 1037–1043.
Olley, J., Burton, J., Smolders, K., Pantus, F., Pietsch, T., 2012. The application of fallout radionuclides to determine the dominant erosion process in water supply catchments of subtropical south-east Queensland, Australia. Hydrol. Process. 27, 885–895.
Olley, J., Brooks, A., Spencer, J., Pietsch, T., Borombovits, D., 2013. Subsoil erosion dominates the supply of fine sediment draining into Princess Charlotte Bay, Australia. J. Environ. Radioact. 124, 121–129.
Olsen, C.R., Larsen, I.L., Lowry, P.D., Cutshall, N.H., Todd, J.F., Wong, G.T.F., Casey, W.H., 1985. Atmospheric fluxes and marsh-soil inventories of ^{7}Be and ^{210}Pb. J. Geophys. Res. Atmos. 90 (D6), 10487–10495.
Patin, J., Mouche, E., Ribolzi, O., Chaplot, V., Sengtahevanghoung, O., Latsachak, K.O., Soulileuth, B., Valentin, C., 2012. Analysis of runoff production at the plot scale during a long-term survey of a small agricultural catchment in Lao PDR. J. Hydrol. 426–427, 79–92.
Pilgrim, D.H., Huff, D.D., Steele, T.D., 1979. Use of specific conductance and contact time relations for separating flow components in storm runoff. Water Resour. Res. 15, 329–339.
Reyss, J.-L., Schmidt, S., Legeleux, F., Bonté, P., 1995. Large low background well-type detectors for measurements of environmental radioactivity. Nucl. Instrum. Methods Phys. Res. Sect. A Accel. Spectrometers Detect. Assoc. Equip. 357, 391–397.
Ribolzi, O., Vallès, V., Bariac, T., 1996. Comparison of hydrograph deconvolutions using residual alkalinity, chloride, and oxygen-18 as hydrochemical tracers. Water Res. Res. 32, 1051–1059.
Ribolzi, O., Cuny, J., Sengsoulichanh, P., Pierret, A., Thiebaux, J.P., Huon, S., Bourdon, E., Robain, H., Sengtaheuangoung, O., 2008. Assessment of water quality along a tributary of the Mekong River in a mountainous, mixed land-use environment of the Lao P.D.R. Lao J. Agric. For. 17, 91–111.
Ribolzi, O., Cuny, J., Sengsoulichanh, P., Mousquès, C., Soulileuth, B., Pierret, A., Huon, S., Sengtaheuanghoung, O., 2010. Land use and water quality along a Mekong tributary in Northern Lao P.D.R. Environ. Manage. 47, 291–302.
Ribolzi, O., Patin, J., Bresson, L.M., Latsachack, K.O., Mouche, E., Sengtaheuanghoung, O., Silvera, N., Thiébaux, J.P., Valentin, C., 2011. Impact of slope gradient on soil surface features and infiltration on steep slopes in northern Laos. Geomorphology 127, 53–63.
Ritchie, J.C., McCarty, G.W., 2003. ^{137}Cesium and soil carbon in a small agricultural watershed. Soil Tillage Res. 69, 45–51.
Ritchie, J.C., McHenry, J.R., 1990. Application of radioactive fallout cesium-137 for measuring soil erosion and sediment accumulation rates and patterns: a review. J. Environ. Qual. 19, 215–233.
Rumpel, C., Kögel-Knabner, I., 2011. Deep soil organic matter – a key but poorly understood component of terrestrial C cycle. Plant Soil 338, 143–158.
Saari, H.-K., Schmidt, S., Castaing, P., Blanc, G., Sautour, B., Masson, O., Cochran, J.K., 2010. The particulate ^{7}Be/^{210}Pb$_{xs}$ and ^{234}Th/^{210}Pb$_{xs}$ activity ratios as tracers for tidal-to-seasonal particle dynamics in the Gironde estuary (France): implications for the budget of particle-associated contaminants. Sci. Total Environ. 408, 4784–4794.
Schindler Wildhaber, Y., Liechti, R., Alewell, C., 2012. Organic matter dynamics and stable isotope signature as tracers of the sources of suspended sediment. Biogeosciences 9, 1985–1996.
Sidle, R.C., Ziegler, A.D., Negishi, J.N., Nik, A.R., Siew, R., Turkelboom, F., 2006. Erosion processes in steep terrain—truths, myths, and uncertainties related to forest management in Southeast Asia. For. Ecol. Manage. 224, 199–225.
Sklash, M.G., Farvolden, R.N., 1979. The role of groundwater in storm runoff. J. Hydrol. 43, 45–65.
Smith, J.C., Galy, A., Hovius, N., Tye, A.M., Turowski, J.M., Schleppi, P., 2013. Runoff-driven export of particulate organic carbon from soil in temperate forested uplands. Earth Planet. Sci. Lett. 365, 198–208.
Taylor, A., Blake, W.H., Couldrick, L., Keith-Roach, M.J., 2012. Sorption behaviour of beryllium-7 and implications for its use as a sediment tracer. Geoderma 187–188, 16–23.
UNESCO (United Nations Educational Scientific and Cultural Organization) 1974. FAO/UNESCO Soil map of the world, 1: 5,000,000 Vol.1, Paris: UNESCO.
VKL (Viêt-nam-Kampuchia-Lào) geological map 1971. Reviewed and completed by Fontaine H. 3rd edition. Direction Géographique Nationale du Vietnam, Dalat.
Valentin, C., Agus, F., Alamban, R., Boosaner, A., Bricquet, J.-P., Chaplot, V., de Guzman, T., de Rouw, A., Janeau, J.-L., Orange, D., Phachomphonh, K., Podwojewski, P., Ribolzi, O., Silvera, N., Subagyono, K., Thiébaux, J.-P., Vadari, T., 2008. Runoff and sediment losses from 27 upland catchments in Southeast Asia: impact of rapid land use changes and conservation practices. Agric. Ecosyst. Environ. 128, 225–238.